ACS Energy LETTERS

http://pubs.acs.org/journal/aelccp

Interplay of Kinetic and Thermodynamic Reaction Control Explains Incorporation of Dimethylammonium Iodide into $CsPbI_3$

Aditya Mishra, Dominik J. Kubicki,* Ariadni Boziki, Rohit D. Chavan, Mathias Dankl, Marko Mladenović, Daniel Prochowicz, Clare P. Grey, Ursula Rothlisberger,* and Lyndon Emsley*

Cite This: *ACS Energy Lett.* 2022, 7, 2745−2752

Read Online

ACCESS | Metrics & More | Article Recommendations | Supporting Information

ABSTRACT: **$CsPbI_3$ is a promising material for optoelectronics owing to its thermal robustness and favorable bandgap. However, its fabrication is challenging because its photoactive phase is thermodynamically unstable at room temperature. Adding dimethylammonium (DMA) alleviates this instability and is currently understood to result in the formation of $DMA_xCs_{1-x}PbI_3$ perovskite solid solutions. Here, we use NMR of the ^{133}Cs and ^{13}C local structural probes to show that these solid solutions are not thermodynamically stable, and their synthesis under thermodynamic control leads to a segregated mixture of yellow one-dimensional $DMAPbI_3$ phase and δ-$CsPbI_3$. We show that mixed-cation $DMA_xCs_{1-x}PbI_3$ perovskite phases only form when they are kinetically trapped by rapid antisolvent-induced crystallization. We explore the energetics of DMA incorporation into $CsPbI_3$ using first-principles calculations and molecular dynamics simulations and find that this process is energetically unfavorable. Our results provide a complete atomic-level picture of the mechanism of DMA-induced stabilization of the black perovskite phase of $CsPbI_3$ and shed new light on this deceptively simple material.**

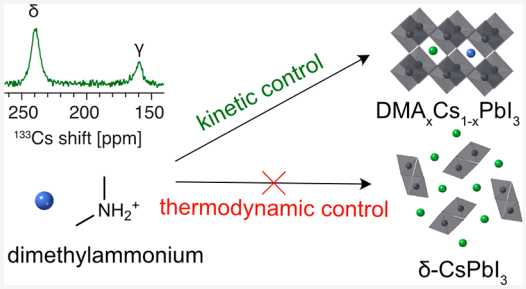

Organic−inorganic halide perovskite solar cells (PSCs) have been developed within a decade to achieve remarkable power conversion efficiencies (PCEs) of over 25%.[1,2] However, their thermal stability has been a major bottleneck due to the volatility of the organic components at elevated temperatures, which leads to irreversible degradation of device performance over time.[3−7] All-inorganic PSCs based on cesium lead halides have attracted significant attention owing to their higher thermal stability and have reached PCEs on the order of 20%, albeit typically with various organic additives.[8−16] $CsPbI_3$ has been identified as one of the most promising solar cell materials due to its bandgap (E_g = 1.71 eV) which is close to the radiative efficiency limit.[8,17] However, its perovskite α phase ($Pm\bar{3}m$) is thermodynamically stable only above ca. 300 °C. On cooling, it transforms first to the tetragonal β phase ($P4/mbm$) and then the orthorhombic γ phase ($Pbnm$) with distorted corner-sharing octahedra (Figure 1A).[8,18,19] The γ phase is metastable at room temperature and readily transforms to an orthorhombic nonperovskite δ-phase ($Pnma$). The metastable perovskite phase (γ-$CsPbI_3$) has been stabilized using several strategies to date to enable its use in optoelectronic devices. These strategies include incorporating Br^- and F^-;[13,16,20−22] solvent-controlled growth;[23,24] the use of intermediate phases;[25] doping with metal ions such as Bi^{3+},[26,27] Sn^{2+},[21] Sb^{2+},[28] and Eu^{2+};[16,29] passivation with small organic molecules;[30−32] and addition of hydroiodic acid (HI) to the precursor solution.[33−35] The last strategy has been remarkably successful and has been adopted as the primary method to fabricate all-inorganic PSCs based on $CsPbI_3$.[36−38] In 2018, Ke et al. reported that the addition of HI catalyzes the acidic hydrolysis of the commonly used solvent, dimethylformamide (DMF), leading to dimethylammonium (DMA) as a degradation product. DMA was thought to incorporate into the perovskite structure as an A-site cation leading to $DMA_xCs_{1-x}PbI_3$ phases.[34] Further, Wang et al. showed that DMA can affect $CsPbI_3$ crystallization kinetics and thin film morphology.[38] DMA has also been used in hybrid PSCs in an attempt to modulate electronic properties,[39] stability,[36−38,40] and efficiency.[34,36−38] However, the speciation and microscopic mechanism of action of DMA in mixtures with $CsPbI_3$

Received: April 14, 2022
Accepted: July 15, 2022
Published: July 26, 2022

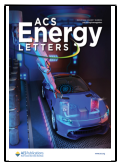

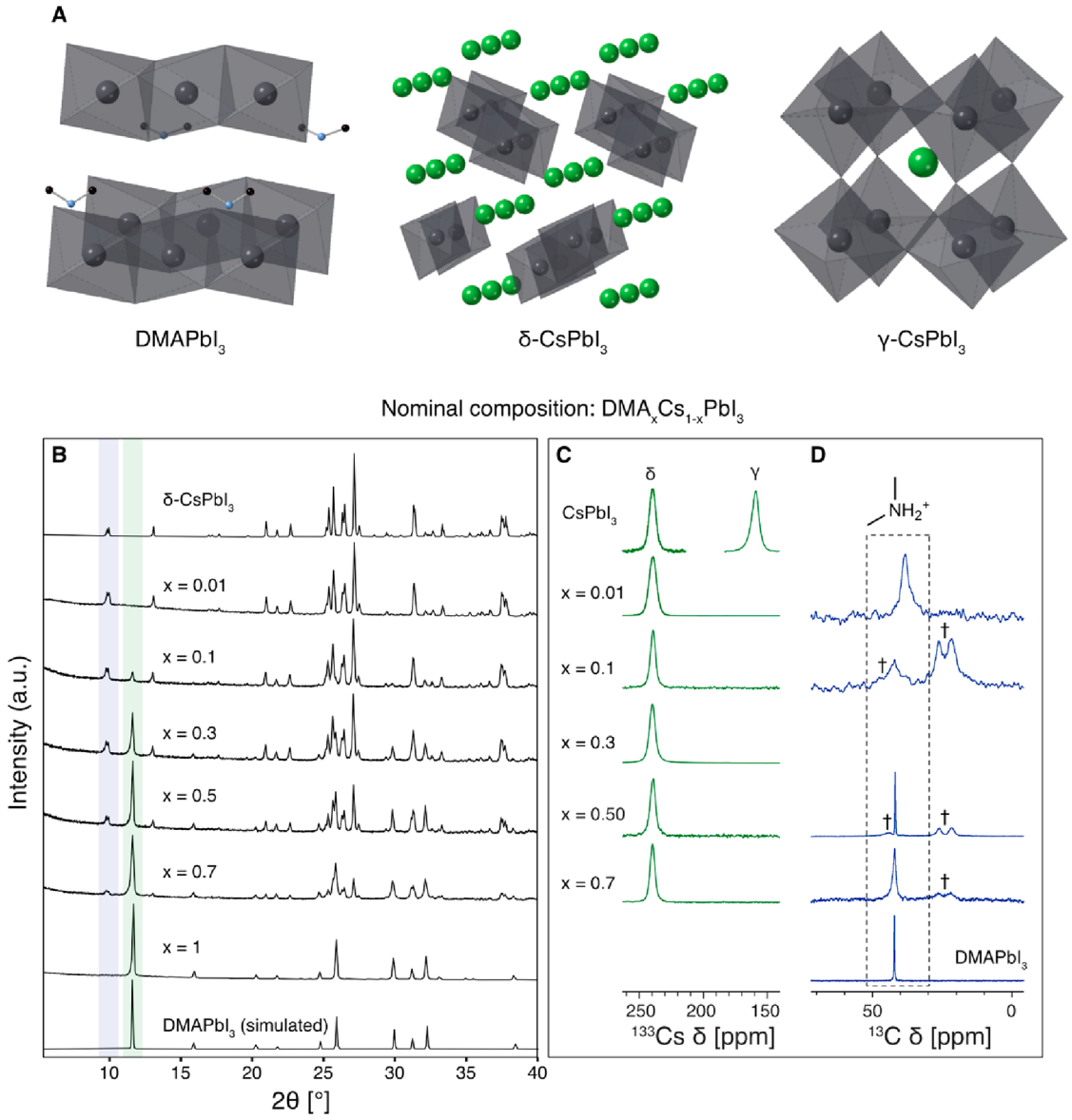

Figure 1. Characterization of the $DMA_xCs_{1-x}PbI_3$ materials. (A) Crystal structures of the compositional end members showing the PbI_6 connected octahedra in gray, Cs^+ in green, and DMA cations (C, black; N, blue); (B) powder XRD (see Figure S2 for enlarged view), (C) ^{133}Cs MAS, and (D) $^1H-^{13}C$ CPMAS solid-state NMR spectra. All experiments were carried out at room temperature (ca. 294 K). The NMR spectrum of the $x = 0.01$ material was recorded using a Hahn echo to avoid baseline distortions. † indicates trace (<2 wt % based on the ^1H spectrum) polypropylene (PP) used as the grinding jar material, peaks at 21.5, 26.1, and 44.3 ppm. The $x = 0.01$ material was ground in an agate jar to avoid PP contamination. The full ^{133}Cs spectra and further experimental details are given in Figure S1 and Tables S1 and S3.

in the solid state have been elusive. More recently, Marshall et al. concluded that mixed-cation $DMA_xCs_{1-x}PbI_3$ phases form using a combination of optical spectroscopies and XRD.[41] Recent progress in characterizing the role of DMA in perovskite solar cells has recently been reviewed.[62] While those techniques provide insight into the long-range structure and bulk properties of materials, there is a critical need to investigate the local structure of the individual components to assess their structure and role at the atomic level.

Solid-state NMR spectroscopy has emerged as a powerful local structure characterization technique to determine the speciation of dopants.[42−44] Here, we use it to show that the formation of mixed-cation iodoplumbates of DMA and Cs, i.e., compositions with the nominal formula $DMA_xCs_{1-x}PbI_3$, is determined by an interplay of kinetic and thermodynamic reaction control factors. We experimentally show that thermodynamic reaction conditions (mechanosynthesis, solution processing without an antisolvent) lead to materials completely segregated into δ-$CsPbI_3$ and $DMAPbI_3$, while kinetic reaction control (spin coating with rapid crystallization induced by antisolvent dripping) leads to a mixed-cation solid solution. From this, we conclude that the atomic-level mechanism of γ-$CsPbI_3$ stabilization with DMAI in thin films processed with an antisolvent involves incorporation of DMA into the perovskite structure. We elucidate and rationalize the composition of the resulting materials using a combination of long-range (X-ray diffraction) and local structure (solid-state NMR) probes and density functional theory (DFT)-based calculations and molecular dynamics (MD) simulations.

We first focus our attention on compositions corresponding to the nominal formula $DMA_xCs_{1-x}PbI_3$ (x = 0.01, 0.10, 0.30, 0.50, 0.70, 1.0) prepared using solid-state mechanosynthesis

https://doi.org/10.1021/acsenergylett.2c00877
ACS Energy Lett. 2022, 7, 2745−2752

followed by annealing at 100 °C (see Methods in the SI). All of the resulting polycrystalline powders were yellow. Powder X-ray diffraction (pXRD) data show that the mixed DMA/Cs samples are mixtures of two nonperovskite hexagonal phases: $DMAPbI_3$ and δ-$CsPbI_3$ (Figure 1B). The composition-dependent evolution can be readily followed in the 2θ = 9–12° region where δ-$CsPbI_3$ yields reflections at 9.8° and 10.0°, while $DMAPbI_3$ has a reflection at 11.6°. The diffractograms of mixed DMA/Cs compositions correspond to mixtures of δ-$CsPbI_3$ and $DMAPbI_3$, with no new mixed-cation phases being present.

To gain a more detailed picture of Cs/DMA mixing, we elucidate the local structure of Cs and DMA using magic-angle-spinning (MAS) ^{133}Cs and ^{13}C solid-state NMR, respectively. ^{133}Cs NMR is particularly useful for studying Cs-containing metal halide perovskites (MHPs) as it can be used to evidence Cs incorporation into hybrid MHPs[46] since its shift strongly depends on the structure topology and halide composition.[45] Figure 1C shows the ^{133}Cs MAS NMR spectra of the materials. The reference $CsPbI_3$ sample was annealed at 300 °C before the measurement to capture the metastable γ perovskite phase (158 ppm). The transformation back to the orthorhombic δ phase (240 ppm) occurs on the time scale of minutes (half-life of γ-$CsPbI_3$ at RT is about 30 min),[45] so it possible to record a high-quality spectrum of each phase by taking a measurement immediately after annealing (phase-pure γ-$CsPbI_3$) and after a few hours (phase-pure δ-$CsPbI_3$). For comparison, a spectrum of this material midtransition is shown as a reference in Figure 2A. ^{133}Cs spectra of the compositions formally denoted as $DMA_xCs_{1-x}PbI_3$ (x = 0.01, 0.1, 0.3, 0.5, 0.7) show a single peak corresponding to δ-$CsPbI_3$ with no substantial shift or line width variation as a function of the DMA/Cs ratio (see also Table S1). The γ phase was not detected in any of the samples, consistent with their yellow appearance. To elucidate the speciation of DMA, we recorded room-temperature ^{13}C cross-polarization (CP) MAS NMR spectra (Figure 1D). While the ^{13}C chemical shift of DMA in the $DMA_xCs_{1-x}PbI_3$ (x = 0.1, 0.3, 0.5, 0.7) compositions is consistent with it being present as $DMAPbI_3$, in agreement with the XRD data, we found remarkable variation in line width, which is uncorrelated with the DMA/Cs ratio (Table S2). For example, the line widths are 0.224 ± 0.006 ppm for $DMAPbI_3$, 1.35 ± 0.03 ppm for $DMA_{0.7}Cs_{0.3}PbI_3$, and 3.48 ± 0.04 ppm for $DMA_{0.01}Cs_{0.99}PbI_3$. Since broader line widths correspond to more disordered local environments, we attribute this effect to the presence of nanosized regions and disorder of $DMAPbI_3$ formed as a result of mechanosynthesis. Interestingly, in the case of the x = 0.01 material, the ^{13}C signal of DMA is shifted to lower frequencies, indicating a substantially different local environment. This effect may result from the interaction of the nanosized grains of $DMAPbI_3$ with the surface of δ-$CsPbI_3$ owing to the high level of dispersion of the hybrid phase within the all-inorganic matrix. The effect is only visible in the most dilute material where we recorded the ^{13}C spectrum over 214 h. We suggest that this effect could be further investigated using surface-enhanced NMR spectroscopy.[51] Taken together, these XRD and solid-state NMR results show that DMA has no propensity to form thermodynamically stable mixed-cation phases with $CsPbI_3$ and instead forms $DMAPbI_3$, i.e., the two cations do not mix at the atomic level. However, the formation of a black perovskite phase in this phase diagram has been repeatedly reported by multiple groups using solution synthesis,[33,34] which led us to

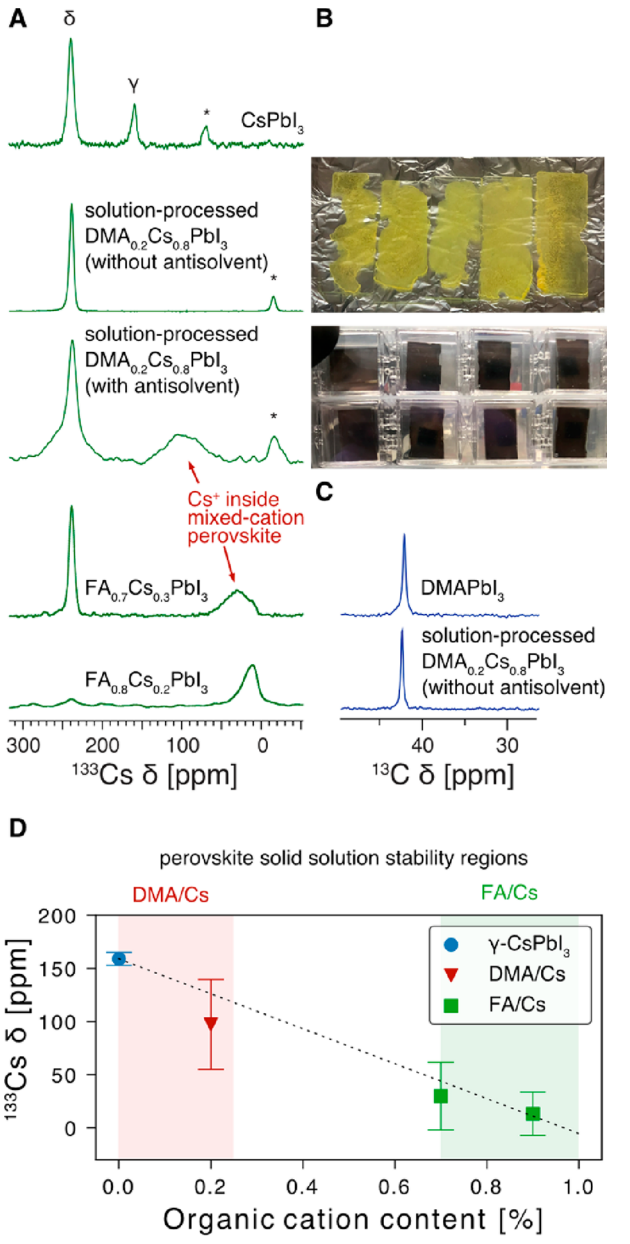

Figure 2. Characterization of $DMA_{0.2}Cs_{0.8}PbI_3$ materials prepared by solution processing. (A) ^{133}Cs MAS solid-state NMR spectra of $DMA_{0.2}Cs_{0.8}PbI_3$ made with and without the use of an antisolvent (chlorobenzene). Rapid antisolvent-induced crystallization leads to kinetic trapping of a mixed-cation perovskite with DMA incorporated into the perovskite structure. Its NMR signature its similar to that previously observed for $FA_xCs_{1-x}PbI_3$ solid solutions (Adapted with permission from *J. Am. Chem. Soc.* 2017, *139* (40), 14173−14180. Copyright 2017, American Chemical Society). Asterisks indicate spinning sidebands. (B) Photographs of films made with and without the use of an antisolvent. (C) $^{1}H-^{13}C$ CPMAS solid-state NMR spectrum of $DMA_{0.2}Cs_{0.8}PbI_3$ showing that DMA is only present as $DMAPbI_3$. All experiments were carried out at room temperature (ca. 294 K). (D) Correlation between the ^{133}Cs shift of black perovskite solid solutions of $A_xCs_{1-x}PbI_3$ where A = DMA and FA. The error bars are taken as the corresponding full width at half-maximum (fwhm) values. The solid-solution stability regions are indicated based on refs 41 and 46. The linear weighed regression equation is δ_{Cs} [ppm] = −164x + 159. Further experimental details are given in Figure S1 and Tables S2 and S3.

https://doi.org/10.1021/acsenergylett.2c00877
ACS Energy Lett. 2022, 7, 2745−2752

investigate solution-processed $DMA_{0.20}Cs_{0.80}PbI_3$. We chose this composition because it has a high DMA/Cs ratio while still falling within the stability range of the solid solution reported by Marshall et al.[41] While we have previously shown that qualitative chemical reactivity tends to be identical in solution and mechanosynthesized materials,[46,47] it appears that in this case solution processing is key to the formation of the black perovskite phase. We first attempted to make the solution-processed material by drop casting without the use of an antisolvent, and it behaved in analogy to the materials made by mechanosynthesis; i.e., we observed complete phase segregation into δ-$CsPbI_3$ and $DMAPbI_3$ (Figure 2A,C). However, all previous works reporting DMA-assisted formation of a stable black phase used an antisolvent in their deposition process. The role of an antisolvent is to induce rapid crystallization of an intermediate phase by reducing its solubility, which is transformed into the perovskite phase during annealing. Those results suggested to us that the use of an antisolvent may be key to understanding the CsI-DMAI-PbI_2 phase diagram. After optimizing the deposition process (see the Experimental Section in the SI for details), we found that chlorobenzene reproducibly yields black films, which are stable, if humidity is strictly excluded (Figure 2B). The ^{133}Cs MAS NMR spectrum of this black form shows a new very broad peak centered at about 100 ppm with a line width of 42 ppm (Figure 2A). This NMR signature is reminiscent of Cs^+ incorporated into $FAPbI_3$ (Figure 2A, bottom), with the remarkably large line width resulting from substantial static disorder, i.e., the presence of a distribution of different nearest and next-nearest neighbor local environments. For example, in the cubic perovskite aristotype $CsPbI_3$, Cs has six nearest neighbors at 6.3 Å (neighboring cubooctahedra), 12 nearest neighbors at 8.9 Å (across the $[PbI_6]^{4-}$ vertices), and eight more at 10.9 Å (across the $[PbI_6]^{4-}$ octahedra). Including all the next-nearest neighbors within the 20 Å radius, it has a total of 146 Cs^+ ions surrounding it, each of which can be replaced by DMA, leading to a slight change in ^{133}Cs shift. The convolution of these possibilities leads to the experimentally observed broad line shape. Despite all of the precautions taken (handling inside an argon glovebox, transfer of the rotor in an airtight Schlenk flask, spinning using dry nitrogen), we found that this phase disappears within 3−4 h of starting the measurement. Figure S3 shows the evolution of this spectrum as a function of time. We were unable to record a ^{13}C spectrum of this material (no signal after 8 h of acquisition), presumably because of the small amount of material and substantial disorder of the degraded phase leading to signal broadening. The spectrum shown in Figure 2A is a sum of spectra taken during the first 8 h of the measurement. Another interesting aspect of this spectrum is that the signal corresponding to δ-$CsPbI_3$ has a broad underlying component, which corresponds to a δ-$CsPbI_3$ in which some Cs was replaced by DMA. This result is similar to what we have previously observed in Cs-rich $FAPbI_3$ compositions such as $FA_{0.16}Cs_{0.84}PbI_3$.[48] These results evidence that DMA can be incorporated into the perovskite phase of $CsPbI_3$, with the prerequisite being fast antisolvent-induced crystallization, which leads to kinetic stabilization of the metastable phase. On the other hand, when the material is prepared under thermodynamic conditions (mechanosynthesis, slow solvent evaporation), complete phase segregation into δ-$CsPbI_3$ and $DMAPbI_3$ results. This behavior contrasts with that observed for Cs/FA and Cs/GUA, which yield mixed-cation iodoplumbate phases under thermodynamic conditions.[46,48,49,61] The importance of kinetic reaction control also has potential bearing on the role and speciation of Rb^+ and K^+ in hybrid MHPs doped with these cations, where we have previously observed complete segregation of the inorganic dopants under thermodynamic control.[46,50] It is also noteworthy that the overall structure topology affects the incorporation of small organic cations into halide perovskite cages. For example, while large cations, such as DMA and GUA do not form 3D perovskites on their own owing to their large size, they can be incorporated into the cubooctahedral space in 2D/3D Ruddlesden−Popper phases.[63−65] The lack of thermodynamic stability of Cs/DMA iodoplumbate phases can be rationalized by the difference in ionic radii of Cs and DMA. The smaller Cs is replaced by the larger DMA, imposing distortions in the lattice. On increasing the DMA/Cs ratio, the volume of the unit cell is expected to increase proportionally. On the one hand, the incorporation of DMA alleviates the initial strain in γ-$CsPbI_3$. On the other, because of the antibonding character of the valence band maximum, the reduction of the lattice distortion leads to an increase in the overlap of the I p and Pb s orbitals, which in turn leads to destabilization of the mixed-cation perovskite phase. We have previously also observed this phenomenon in Cs-rich $Cs_xFA_{1-x}PbI_3$ solid solutions.[48] For reference, on the basis of Bader volume calculations, DMA has an effective radius of 2.67 A, while MA and FA have effective radii of 2.37 and 2.48 Å, respectively. Guanidinium (GUA), which has been shown to form mixed GUA/MA and GUA/FA 3D perovskite phases, has an effective radius of 2.68 Å.[61] Finally, we also noticed that the ^{133}Cs shift of the Cs^+ inside the perovskite phase is correlated with the content of the organic cation present in the solid solution (Figure 2D). There are two regions corresponding to stable $A_xCs_{1-x}PbI_3$ solid solutions: 0−25 mol % (A = DMA, kinetic stability) and >70 mol % (A = FA, thermodynamic stability). Interestingly, there are currently no known organic cations that lead to stable $A_xCs_{1-x}PbI_3$ phases for x in the 25−70 mol % range.

To gain further insight into the potential miscibility of DMA and Cs iodoplumbates, we next studied their mixing free energy using DFT calculations.[52,53] We used the Perdew−Burke−Ernzerhof (PBE) functional[54] to determine the relative stability of perovskite and nonperovskite phases of hypothetical $DMA_xCs_{1-x}PbI_3$ mixtures at 0 K with up to 50 mol % of Cs replaced by DMA according to

$$\Delta E_{\text{phase}}(DMA_xCs_{1-x}PbI_3) = E_{\text{phase}}(DMA_xCs_{1-x}PbI_3) - [xE_{\text{phase}}(DMAPbI_3) + (1-x)E_{\text{phase}}(CsPbI_3)]$$

We found that the energy difference between various substitution patterns at any concentration is only on the order of 0.01 eV per stoichiometric unit for both the γ and δ phases. This small amount justifies the use of the analytical formula for ideal alloys to estimate the mixing entropy contribution to the free energy.[55]

$$T\Delta S_{\text{mix}} = -k_B T \sum_{i=1}^{n} c_i \ln(cli)$$

where k_B is the Boltzmann constant, T is the temperature, n is the number of components, and c_i is the atomic fraction of

https://doi.org/10.1021/acsenergylett.2c00877
ACS Energy Lett. 2022, 7, 2745−2752

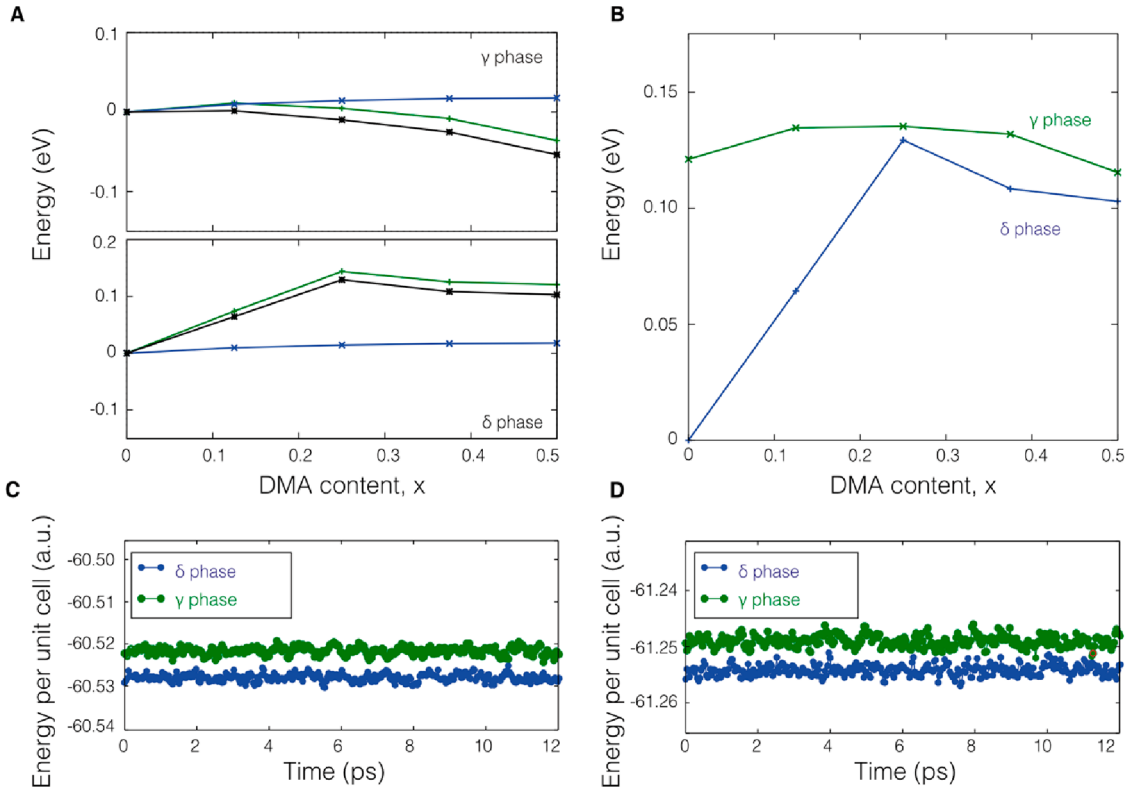

Figure 3. Energetics of Cs/DMA mixing in the γ and δ phases. (A) Variation of the free energy of mixing expressed as $\Delta F = \Delta E - T\Delta S$ (black line), the internal energy, ΔE (green line), and the mixing entropy contribution, $T\Delta S$ (for T = 298 K, blue line), as a function of the molar fraction of DMA in $DMA_xCs_{1-x}PbI_3$ mixtures for the perovskite and δ phases, respectively. (B) Variation of the free energy of mixing plotted relative to the pure δ phase as a reference. Energies are given per stoichiometric unit. Potential energy per stoichiometric unit for perovskite and δ phases from first-principles MD simulations in a constant-temperature, constant-volume (NVT) ensemble at 300 K for (C) $Cs_{0.625}DMA_{0.375}PbI_3$ and (D) $Cs_{0.5}DMA_{0.5}PbI_3$. The y axis shows energy per stoichiometric unit. Full details of the calculation methods are given in the SI.

component i. In the case of $DMA_xCs_{1-x}PbI_3$ mixtures, the above equation leads to the following:

$$T\Delta S_{\text{phase}}(DMA_xCs_{1-x}PbI_3) = -k_B T[x \ln x + (1-x)\ln(1-x)]$$

where x is the mol % of DMA incorporated into the $CsPbI_3$ structure.

Figure 3A shows the energetic and entropic contributions to the free energy of mixing as a function of x for the two phases. For the γ phase and low DMA molar fractions, the replacement of Cs with DMA induces a negligible or slightly positive energetic contribution on the order of 0.01 eV per stoichiometric unit, i.e., energies on the same order of magnitude as the variations between different substitution patterns. Since the values of the mixing free energy for molar fractions of DMA below 37.5 mol % lie within the intrinsic error of the calculations, it is not possible to unambiguously conclude if DMA/Cs mixing in the γ phase leads to marginal stabilization relative to the single-cation end members. On the other hand, for DMA fractions larger than 37.5 mol %, both energetic and entropic contributions favor the formation of mixed-cation phases. In contrast, in the δ phase, cation mixing leads to significant energetic destabilization for all $DMA_xCs_{1-x}PbI_3$ compositions. The mixing entropy contribution to the free energy calculated at room temperature (298 K) is not sufficient to compensate for this penalty; i.e., in the δ phase, all mixtures in this molar fraction range are predicted to be unstable with respect to demixing into single-cation phases. For a possible reversion of relative phase stability between the γ and δ-phases in the mixed compounds, the energetic stabilization of the γ phase and the simultaneous destabilization of the δ phase would have to be large enough to compensate for the initial energy penalty between the two phases, which however turns out not to be the case (Figure 3B).

Table 1 shows the relative energetics per stoichiometric unit between the δ and the γ phases at 0 K. The δ phase remains energetically preferred at 0 K, but the energy difference is substantially reduced upon mixing, consistent with the energetic trends in the mixing free energies.

Table 1. Relative Energetics Given by $\Delta E = E_\gamma - E_\delta$ per s.u. of the γ Relative to the δ Phase in $DMA_xCs_{1-x}PbI_3$

x (mol %)	ΔE (eV)
0	0.12
12.5	0.07
25	0.01
37.5	0.02
50	0.01

The stability of mixed component phases at room temperature can be substantially affected by vibrational entropy which is absent in the calculations carried out at 0 K. In the case of lead halide perovskites, the calculation of

https://doi.org/10.1021/acsenergylett.2c00877
ACS Energy Lett. 2022, 7, 2745−2752

vibrational corrections is not trivial and leads to the appearance of imaginary modes in harmonic and quasi-harmonic phonon calculations.[56] This artifact has been addressed by including anharmonic phonon−phonon interactions in halide double perovskites.[57,58] However, in all-inorganic lead halide perovskites, vibrational instabilities are present that are associated with octahedral tilting in the high-temperature phase.[59,60] Consequently, we approached the question of assessing relative phase stabilities at finite temperatures by carrying out direct MD simulations (full details are given in SI). Figure 3C and D show potential energies per stoichiometric unit for γ and δ phases of $Cs_{0.625}DMA_{0.375}PbI_3$ and $Cs_{0.5}DMA_{0.5}PbI_3$ from first-principles MD simulations at 300 K. Figure 3C and D show that the δ phase remains thermodynamically more stable than the perovskite phase even when finite temperature effects are fully taken into account. Given the time scale of first-principles MD simulations (of a few picoseconds) and considering that the systems do not contain any vacancies that might accelerate demixing, no spontaneous phase segregation toward the pure phases is expected to be observed, although the calculated mixing free energies show that all mixtures in the δ-phase are unstable with respect to demixing.

In conclusion, we have assessed the possibility of incorporating DMA into the $CsPbI_3$ lattice using a combination of long-range and local structure probes and static and dynamic first-principles calculations. Our results show a remarkable dependence on the reaction conditions, with kinetic control leading to stabilization of the mixed-cation $DMA_xCs_{1-x}PbI_3$ perovskite phase and thermodynamic control resulting in complete phase segregation into a physical mixture of δ-$CsPbI_3$ and $DMAPbI_3$. These experimental findings are rationalized by DFT calculations, which show that, although cation mixing in the perovskite phase is possible, the overall, thermodynamically most stable phase is the demixed δ-phase. We contend that further multimodal studies into the chemical transformations of $CsPbI_3$ and its solid solutions are urgently needed to improve our understanding of these materials.

■ ASSOCIATED CONTENT

Supporting Information

The Supporting Information is available free of charge at https://pubs.acs.org/doi/10.1021/acsenergylett.2c00877.

Materials and methods and details of the solid-state NMR measurements (PDF)

■ AUTHOR INFORMATION

Corresponding Authors

Dominik J. Kubicki − *Laboratory of Magnetic Resonance, Institut des Sciences et Ingénierie Chimiques, École Polytechnique Fédérale de Lausanne (EPFL), 1015 Lausanne, Switzerland; Department of Physics, University of Warwick, CV4 7AL Coventry, United Kingdom;* orcid.org/0000-0002-9231-6779; Email: dominik.kubicki@warwick.ac.uk

Ursula Rothlisberger − *Laboratory of Computational Chemistry and Biochemistry, Institut des Sciences et Ingénierie Chimiques, École Polytechnique Fédérale de Lausanne (EPFL), 1015 Lausanne, Switzerland;* orcid.org/0000-0002-1704-8591; Email: ursula.roethlisberger@epfl.ch

Lyndon Emsley − *Laboratory of Magnetic Resonance, Institut des Sciences et Ingénierie Chimiques, École Polytechnique Fédérale de Lausanne (EPFL), 1015 Lausanne, Switzerland;* orcid.org/0000-0003-1360-2572; Email: lyndon.emsley@epfl.ch

Authors

Aditya Mishra − *Laboratory of Magnetic Resonance, Institut des Sciences et Ingénierie Chimiques, École Polytechnique Fédérale de Lausanne (EPFL), 1015 Lausanne, Switzerland*

Ariadni Boziki − *Laboratory of Computational Chemistry and Biochemistry, Institut des Sciences et Ingénierie Chimiques, École Polytechnique Fédérale de Lausanne (EPFL), 1015 Lausanne, Switzerland;* orcid.org/0000-0002-2347-8993

Rohit D. Chavan − *Institute of Physical Chemistry, Polish Academy of Sciences, 01-224 Warsaw, Poland*

Mathias Dankl − *Laboratory of Computational Chemistry and Biochemistry, Institut des Sciences et Ingénierie Chimiques, École Polytechnique Fédérale de Lausanne (EPFL), 1015 Lausanne, Switzerland*

Marko Mladenović − *Laboratory of Computational Chemistry and Biochemistry, Institut des Sciences et Ingénierie Chimiques, École Polytechnique Fédérale de Lausanne (EPFL), 1015 Lausanne, Switzerland*

Daniel Prochowicz − *Institute of Physical Chemistry, Polish Academy of Sciences, 01-224 Warsaw, Poland;* orcid.org/0000-0002-5003-5637

Clare P. Grey − *Yusuf Hamied Department of Chemistry, University of Cambridge, Cambridge CB2 1EW, United Kingdom;* orcid.org/0000-0001-5572-192X

Complete contact information is available at: https://pubs.acs.org/10.1021/acsenergylett.2c00877

Notes

The authors declare no competing financial interest.

All data presented here (raw NMR and XRD data, and DFT and MD input files) can be accessed at the following DOI: 10.5281/zenodo.6903645 and it is available under the license CC-BY-4.0 (Creative Commons Attribution-ShareAlike 4.0 International).

■ ACKNOWLEDGMENTS

We thank Zaiwei Wang for discussions and help in designing preliminary experiments. D.J.K. acknowledges the support of the University of Warwick. A.M. and L.E. are grateful for the support from SNSF grant number 200020_178860, and U.R. acknowledges funding from SNSF grant number 200020-185092 and the NCCR MUST. Computing time was provided by the Swiss National Computing Centre CSCS. R.D.C and D.P. acknowledge the National Science Centre (Grant SONATA BIS 10, No. 2020/38/E/ST5/00267) for financial support.

■ REFERENCES

(1) Kojima, A.; Teshima, K.; Shirai, Y.; Miyasaka, T. Organometal Halide Perovskites as Visible-Light Sensitizers for Photovoltaic Cells. *J. Am. Chem. Soc.* **2009**, *131* (17), 6050−6051.

(2) NREL Efficiency Chart. https://www.nrel.gov/pv/cell-efficiency.html (accessed 6 July 2022).

(3) Smecca, E.; Numata, Y.; Deretzis, I.; Pellegrino, G.; Boninelli, S.; Miyasaka, T.; La Magna, A.; Alberti, A. Stability of Solution-Processed $MAPbI_3$ and $FAPbI_3$ Layers. *Phys. Chem. Chem. Phys.* **2016**, *18* (19), 13413−13422.

(4) Conings, B.; Drijkoningen, J.; Gauquelin, N.; Babayigit, A.; D'Haen, J.; D'Olieslaeger, L.; Ethirajan, A.; Verbeeck, J.; Manca, J.; Mosconi, E.; De Angelis, F.; Boyen, H. G. Intrinsic Thermal

Instability of Methylammonium Lead Trihalide Perovskite. *Adv. Energy Mater.* **2015**, *5* (15), 1500477.
(5) Berhe, T. A.; Su, W. N.; Chen, C. H.; Pan, C. J.; Cheng, J. H.; Chen, H. M.; Tsai, M. C.; Chen, L. Y.; Dubale, A. A.; Hwang, B. J. Organometal Halide Perovskite Solar Cells: Degradation and Stability. *Energy Environ. Sci.* **2016**, *9* (2), 323−356.
(6) Dualeh, A.; Gao, P.; Seok, S. Il; Nazeeruddin, M. K.; Grätzel, M. Thermal Behavior of Methylammonium Lead-Trihalide Perovskite Photovoltaic Light Harvesters. *Chem. Mater.* **2014**, *26* (21), 6160−6164.
(7) Boyd, C. C.; Cheacharoen, R.; Leijtens, T.; McGehee, M. D. Understanding Degradation Mechanisms and Improving Stability of Perovskite Photovoltaics. *Chem. Rev.* **2019**, *119* (5), 3418−3451.
(8) Eperon, G. E.; Paternò, G. M.; Sutton, R. J.; Zampetti, A.; Haghighirad, A. A.; Cacialli, F.; Snaith, H. J. Inorganic Caesium Lead Iodide Perovskite Solar Cells. *J. Mater. Chem. A* **2015**, *3* (39), 19688−19695.
(9) Swarnkar, A.; Marshall, A. R.; Sanehira, E. M.; Chernomordik, B. D.; Moore, D. T.; Christians, J. A.; Chakrabarti, T.; Luther, J. M. Quantum Dot−Induced Phase Stabilization of α-$CsPbI_3$ Perovskite for High-Efficiency Photovoltaics. *Science* **2016**, *354* (6308), 92−95.
(10) Lim, S.; Kim, J.; Park, J. Y.; Min, J.; Yun, S.; Park, T.; Kim, Y.; Choi, J. Suppressed Degradation and Enhanced Performance of $CsPbI_3$ Perovskite Quantum Dot Solar Cells via Engineering of Electron Transport Layers. *ACS Appl. Mater. Interfaces* **2021**, *13* (5), 6119−6129.
(11) Wang, Y.; Dar, M. I.; Ono, L. K.; Zhang, T.; Kan, M.; Li, Y.; Zhang, L.; Wang, X.; Yang, Y.; Gao, X.; Qi, Y.; Gratzel, M.; Zhao, Y. Thermodynamically Stabilized β-$CsPbI_3$−Based Perovskite Solar Cells with Efficiencies > 18%. *Science* **2019**, *365* (6453), 591−595.
(12) Ye, Q.; Zhao, Y.; Mu, S.; Ma, F.; Gao, F.; Chu, Z.; Yin, Z.; Gao, P.; Zhang, X.; You, J. Cesium Lead Inorganic Solar Cell with Efficiency beyond 18% via Reduced Charge Recombination. *Adv. Mater.* **2019**, *31* (49), 1905143.
(13) Liu, C.; Li, W.; Zhang, C.; Ma, Y.; Fan, J.; Mai, Y. All-Inorganic $CsPbI_2Br$ Perovskite Solar Cells with High Efficiency Exceeding 13%. *J. Am. Chem. Soc.* **2018**, *140* (11), 3825−3828.
(14) Yoon, S. M.; Min, H.; Kim, J. B.; Kim, G.; Lee, K. S.; Seok, S. Il. Surface Engineering of Ambient-Air-Processed Cesium Lead Triiodide Layers for Efficient Solar Cells. *Joule* **2021**, *5* (1), 183−196.
(15) Liang, J.; Qi, Y. B. Recent Progress on All-Inorganic Metal Halide Perovskite Solar Cells. *Mater. Today Nano* **2021**, *16*, 100143.
(16) Xiang, W.; Wang, Z.; Kubicki, D. J.; Tress, W.; Luo, J.; Prochowicz, D.; Akin, S.; Emsley, L.; Zhou, J.; Dietler, G.; Gratzel, M.; Hagfeldt, A. Europium-Doped $CsPbI_2Br$ for Stable and Highly Efficient Inorganic Perovskite Solar Cells. *Joule* **2019**, *3*, 205−214.
(17) Shockley, W.; Queisser, H. J. Detailed Balance Limit of Efficiency of p-n Junction Solar Cells. *J. Appl. Phys.* **1961**, *32* (3), 510−519.
(18) Stoumpos, C. C.; Kanatzidis, M. G. The Renaissance of Halide Perovskites and Their Evolution as Emerging Semiconductors. *Acc. Chem. Res.* **2015**, *48* (10), 2791−2802.
(19) Steele, J. A.; Jin, H.; Dovgaliuk, I.; Berger, R. F.; Braeckevelt, T.; Yuan, H.; Martin, C.; Solano, E.; Lejaeghere, K.; Rogge, S. M. J.; Notebaert, C.; Vandezande, W.; Janssen, K. P. F.; Goderis, B.; Debroye, E.; Wang, Y.-K.; Dong, Y.; Ma, D.; Saidaminov, M.; Tan, H.; Lu, Z.; Dyadkin, V.; Chernyshov, D.; Van Speybroeck, V.; Sargent, E. H.; Hofkens, J.; Roeffaers, M. B. J. Thermal Unequilibrium of Strained Black $CsPbI_3$ Thin Films. *Science* **2019**, *365* (6454), 679−684.
(20) Bian, H.; Bai, D.; Jin, Z.; Wang, K.; Liang, L.; Wang, H.; Zhang, J.; Wang, Q.; Liu, S. Graded Bandgap $CsPbI_{2+x}Br_{1-x}$ Perovskite Solar Cells with a Stabilized Efficiency of 14.4%. *Joule* **2018**, *2* (8), 1500−1510.
(21) Liang, J.; Zhao, P.; Wang, C.; Wang, Y.; Hu, Y.; Zhu, G.; Ma, L.; Liu, J.; Jin, Z. $CsPb_{0.9}Sn_{0.1}IBr_2$ Based All-Inorganic Perovskite Solar Cells with Exceptional Efficiency and Stability. *J. Am. Chem. Soc.* **2017**, *139* (40), 14009−14012.
(22) Fu, L.; Zhang, Y.; Chang, B.; Li, B.; Zhou, S.; Zhang, L.; Yin, L. A Fluorine-Modulated Bulk-Phase Heterojunction and Tolerance Factor for Enhanced Performance and Structure Stability of Cesium Lead Halide Perovskite Solar Cells. *J. Mater. Chem. A* **2018**, *6* (27), 13263−13270.
(23) Ramadan, A. J.; Rochford, L. A.; Fearn, S.; Snaith, H. J. Processing Solvent-Dependent Electronic and Structural Properties of Cesium Lead Triiodide Thin Films. *J. Phys. Chem. Lett.* **2017**, *8* (17), 4172−4176.
(24) Wang, P.; Zhang, X.; Zhou, Y.; Jiang, Q.; Ye, Q.; Chu, Z.; Li, X.; Yang, X.; Yin, Z.; You, J. Solvent-Controlled Growth of Inorganic Perovskite Films in Dry Environment for Efficient and Stable Solar Cells. *Nat. Commun.* **2018**, *9*, 2225.
(25) Zhang, J.; Wang, Z.; Mishra, A.; Yu, M.; Shasti, M.; Tress, W.; Kubicki, D. J.; Avalos, C. E.; Lu, H.; Liu, Y.; Carlsen, B. I.; Agarwalla, A.; Wang, Z.; Xiang, W.; Emsley, L.; Zhang, Z.; Grätzel, M.; Guo, W.; Hagfeldt, A. Intermediate Phase Enhances Inorganic Perovskite and Metal Oxide Interface for Efficient Photovoltaics. *Joule* **2020**, *4* (1), 222−234.
(26) Hu, Y.; Bai, F.; Liu, X.; Ji, Q.; Miao, X.; Qiu, T.; Zhang, S. Bismuth Incorporation Stabilized α-$CsPbI_3$ for Fully Inorganic Perovskite Solar Cells. *ACS Energy Lett.* **2017**, *2* (10), 2219−2227.
(27) Ge, S.; Wang, Y.; Xiang, Z.; Cui, Y. Reset Voltage-Dependent Multilevel Resistive Switching Behavior in $CsPb_{1-x}Bi_xI_3$ Perovskite-Based Memory Device. *ACS Appl. Mater. Interfaces* **2018**, *10* (29), 24620−24626.
(28) Xiang, S.; Li, W.; Wei, Y.; Liu, J.; Liu, H.; Zhu, L.; Chen, H. The Synergistic Effect of Non-Stoichiometry and Sb-Doping on Air-Stable α-$CsPbI_3$ for Efficient Carbon-Based Perovskite Solar Cells. *Nanoscale* **2018**, *10* (21), 9996−10004.
(29) Jena, A. K.; Kulkarni, A.; Sanehira, Y.; Ikegami, M.; Miyasaka, T. Stabilization of α-$CsPbI_3$ in Ambient Room Temperature Conditions by Incorporating Eu into $CsPbI_3$. *Chem. Mater.* **2018**, *30* (19), 6668−6674.
(30) Wang, Y.; Zhang, T.; Kan, M.; Li, Y.; Wang, T.; Zhao, Y. Efficient α-$CsPbI_3$ Photovoltaics with Surface Terminated Organic Cations. *Joule* **2018**, *2* (10), 2065−2075.
(31) Wang, Y.; Zhang, T.; Kan, M.; Zhao, Y. Bifunctional Stabilization of All-Inorganic α-$CsPbI_3$ Perovskite for 17% Efficiency Photovoltaics. *J. Am. Chem. Soc.* **2018**, *140* (39), 12345−12348.
(32) Zhang, T.; Dar, M. I.; Li, G.; Xu, F.; Guo, N.; Grätzel, M.; Zhao, Y. Bication Lead Iodide 2D Perovskite Component to Stabilize Inorganic α-$CsPbI_3$ Perovskite Phase for High-Efficiency Solar Cells. *Sci. Adv.* **2017**, *3* (9), 1−7.
(33) Wang, Y.; Dar, M. I.; Ono, L. K.; Zhang, T.; Kan, M.; Li, Y.; Zhang, L.; Wang, X.; Yang, Y.; Gao, X.; Qi, Y.; Gratzel, M.; Zhao, Y. Thermodynamically Stabilized β-$CsPbI_3$−Based Perovskite Solar Cells with Efficiencies > 18%. *Science* **2019**, *365* (6453), 591−595.
(34) Ke, W.; Spanopoulos, I.; Stoumpos, C. C.; Kanatzidis, M. G. Myths and Reality of $HPbI_3$ in Halide Perovskite Solar Cells. *Nat. Commun.* **2018**, *9* (1), DOI: 10.1038/s41467-018-07204-y.
(35) Daub, M.; Hillebrecht, H. On the Demystification of "$HPbI_3$" and the Peculiarities of the Non-Innocent Solvents H_2O and DMF. *Zeitschrift fur Anorg. und Allg. Chemie* **2018**, *644* (22), 1393−1400.
(36) Bian, H.; Wang, H.; Li, Z.; Zhou, F.; Xu, Y.; Zhang, H.; Wang, Q.; Ding, L.; Liu, S.; Jin, Z. Unveiling the Effects of Hydrolysis-Derived DMAI/$DMAPbI_x$ Intermediate Compound on the Performance of $CsPbI_3$ Solar Cells. *Adv. Sci.* **2020**, *7* (9), 1902868.
(37) Chen, H.; Wei, Q.; Saidaminov, M. I.; Wang, F.; Johnston, A.; Hou, Y.; Peng, Z.; Xu, K.; Zhou, W.; Liu, Z.; Qiao, L.; Wang, X.; Xu, S.; Li, J.; Long, R.; Ke, Y.; Sargent, E. H.; Ning, Z. Efficient and Stable Inverted Perovskite Solar Cells Incorporating Secondary Amines. *Adv. Mater.* **2019**, *31* (46), 1903559.
(38) Wang, Y.; Liu, X.; Zhang, T.; Wang, X.; Kan, M.; Shi, J.; Zhao, Y. The Role of Dimethylammonium Iodide in $CsPbI_3$ Perovskite Fabrication: Additive or Dopant? *Angew. Chem.* **2019**, *131* (46), 16844−16849.
(39) Eperon, G. E.; Stone, K. H.; Mundt, L. E.; Schloemer, T. H.; Habisreutinger, S. N.; Dunfield, S. P.; Schelhas, L. T.; Berry, J. J.; Moore, D. T. The Role of Dimethylammonium in Bandgap

Modulation for Stable Halide Perovskites. *ACS Energy Lett.* **2020**, *5* (6), 1856−1864.
(40) Hu, Y.; Yan, Z.; Li, M.; Wen, X.; Yang, Y.; Choy, W. C. H.; Lu, H. Observing the Stability Evolution of β-$DMA_xCs_{1-x}PbI_2Br$ through Precursor Incubation. *Org. Electron.* **2020**, *84*, 105800.
(41) Marshall, A. R.; Sansom, H. C.; McCarthy, M. M.; Warby, J. H.; Ashton, O. J.; Wenger, B.; Snaith, H. J. Dimethylammonium: An A-Site Cation for Modifying $CsPbI_3$. *Sol. RRL* **2021**, *5* (1),2000599.
(42) Franssen, W. M. J.; Kentgens, A. P. M. Solid−State NMR of Hybrid Halide Perovskites. *Solid State Nucl. Magn. Reson.* **2019**, *100*, 36−44.
(43) Piveteau, L.; Morad, V.; Kovalenko, M. V. Solid-State NMR and NQR Spectroscopy of Lead-Halide Perovskite Materials. *J. Am. Chem. Soc.* **2020**, *142* (46), 19413−19437.
(44) Kubicki, D. J.; Stranks, S. D.; Grey, C. P.; Emsley, L. NMR Spectroscopy Probes Microstructure, Dynamics and Doping of Metal Halide Perovskites. *Nat. Rev. Chem.* **2021**, *5* (9), 624−645.
(45) Karmakar, A.; Dodd, M. S.; Zhang, X.; Oakley, M. S.; Klobukowski, M.; Michaelis, V. K. Mechanochemical Synthesis of 0D and 3D Cesium Lead Mixed Halide Perovskites. *Chem. Commun.* **2019**, *55* (35), 5079−5082.
(46) Kubicki, D. J.; Prochowicz, D.; Hofstetter, A.; Zakeeruddin, S. M.; Grätzel, M.; Emsley, L. Phase Segregation in Cs-, Rb- and K-Doped Mixed-Cation $(MA)_x(FA)_{1-x}PbI_3$ Hybrid Perovskites from Solid-State NMR. *J. Am. Chem. Soc.* **2017**, *139* (40), 14173−14180.
(47) Ummadisingu, A.; Mishra, A.; Kubicki, D. J.; LaGrange, T.; Dučinskas, A.; Siczek, M.; Bury, W.; Milić, J. V.; Grätzel, M.; Emsley, L. Multi-Length Scale Structure of 2D/3D Dion−Jacobson Hybrid Perovskites Based on an Aromatic Diammonium Spacer. *Small* **2021**, 2104287.
(48) Boziki, A.; Kubicki, D. J.; Mishra, A.; Meloni, S.; Emsley, L.; Grätzel, M.; Rothlisberger, U. Atomistic Origins of the Limited Phase Stability of Cs^+-Rich $FA_xCs_{(1-x)}PbI_3$ Mixtures. *Chem. Mater.* **2020**, *32* (6), 2605−2614.
(49) Nazarenko, O.; Kotyrba, M. R.; Wörle, M.; Cuervo-Reyes, E.; Yakunin, S.; Kovalenko, M. V. Luminescent and Photoconductive Layered Lead Halide Perovskite Compounds Comprising Mixtures of Cesium and Guanidinium Cations. *Inorg. Chem.* **2017**, *56* (19), 11552−11564.
(50) Kubicki, D. J.; Prochowicz, D.; Hofstetter, A.; Zakeeruddin, S. M.; Grätzel, M.; Emsley, L. Phase Segregation in Potassium-Doped Lead Halide Perovskites from ^{39}K Solid-State NMR at 21.1 T. *J. Am. Chem. Soc.* **2018**, *140* (23), 7232−7238.
(51) Rossini, A. J.; Zagdoun, A.; Lelli, M.; Lesage, A.; Copéret, C.; Emsley, L. Dynamic Nuclear Polarization Surface Enhanced NMR Spectroscopy. *Acc. Chem. Res.* **2013**, *46* (9), 1942−1951.
(52) Hohenberg, P.; Kohn, W. Inhomogeneous Electron Gas. *Phys. Rev.* **1964**, *136* (3B), B864−B871.
(53) Kohn, W.; Sham, L. J. Self-Consistent Equations Including Exchange and Correlation Effects. *Phys. Rev.* **1965**, *140* (4A), A1133−A1138.
(54) Perdew, J. P.; Burke, K.; Ernzerhof, M. Generalized Gradient Approximation Made Simple. *Phys. Rev. Lett.* **1996**, *77* (18), 3865−3868.
(55) Fultz, B. Vibrational Thermodynamics of Materials. *Prog. Mater. Sci.* **2010**, *55* (4), 247−352.
(56) Brivio, F.; Frost, J. M.; Skelton, J. M.; Jackson, A. J.; Weber, O. J.; Weller, M. T.; Goñi, A. R.; Leguy, A. M. A.; Barnes, P. R. F.; Walsh, A. Lattice Dynamics and Vibrational Spectra of the Orthorhombic, Tetragonal, and Cubic Phases of Methylammonium Lead Iodide. *Phys. Rev. B - Condens. Matter Mater. Phys.* **2015**, *92* (14), 1−8.
(57) Zhao, X.-G.; Yang, J.-H.; Fu, Y.; Yang, D.; Xu, Q.; Yu, L.; Wei, S.-H.; Zhang, L. Design of Lead-Free Inorganic Halide Perovskites for Solar Cells via Cation-Transmutation. *J. Am. Chem. Soc.* **2017**, *139* (7), 2630−2638.
(58) Zhao, X.-G.; Yang, D.; Sun, Y.; Li, T.; Zhang, L.; Yu, L.; Zunger, A. Cu−In Halide Perovskite Solar Absorbers. *J. Am. Chem. Soc.* **2017**, *139* (19), 6718−6725.
(59) Yang, R. X.; Skelton, J. M.; da Silva, E. L.; Frost, J. M.; Walsh, A. Spontaneous Octahedral Tilting in the Cubic Inorganic Cesium Halide Perovskites $CsSnX_3$ and $CsPbX_3$ (X = F, Cl, Br, I). *J. Phys. Chem. Lett.* **2017**, *8* (19), 4720−4726.
(60) Marronnier, A.; Lee, H.; Geffroy, B.; Even, J.; Bonnassieux, Y.; Roma, G. Structural Instabilities Related to Highly Anharmonic Phonons in Halide Perovskites. *J. Phys. Chem. Lett.* **2017**, *8* (12), 2659−2665.
(61) Kubicki, D. J.; Prochowicz, D.; Hofstetter, A.; Saski, M.; Yadav, P.; Bi, D.; Pellet, N.; Lewiński, J.; Zakeeruddin, S. M.; Grätzel, M.; Emsley, L. Formation of Stable Mixed Guanidinium−Methylammonium Phases with Exceptionally Long Carrier Lifetimes for High-Efficiency Lead Iodide-Based Perovskite Photovoltaics. *J. Am. Chem. Soc.* **2018**, *140* (9), 3345−3351.
(62) Fan, Y.; Wang, X.; Miao, Y.; Zhao, Y. The Chemical Design in High-Performance Lead Halide Perovskite: Additive vs Dopant? *J. Phys. Chem. Lett.* **2021**, *12* (48), 11636−11644.
(63) Fu, Y. Stabilization of Metastable Halide Perovskite Lattices in the 2D Limit. *Adv. Mater.* **2022**, *34* (9), 2108556.
(64) Li, X.; Fu, Y.; Pedesseau, L.; Guo, P.; Cuthriell, S.; Hadar, I.; Even, J.; Katan, C.; Stoumpos, C. C.; Schaller, R. D.; Harel, E.; Kanatzidis, M. G. Negative Pressure Engineering with Large Cage Cations in 2D Halide Perovskites Causes Lattice Softening. *J. Am. Chem. Soc.* **2020**, *142* (26), 11486−11496.
(65) Fu, Y.; Hautzinger, M. P.; Luo, Z.; Wang, F.; Pan, D.; Aristov, M. M.; Guzei, I. A.; Pan, A.; Zhu, X.; Jin, S. Incorporating Large A Cations into Lead Iodide Perovskite Cages: Relaxed Goldschmidt Tolerance Factor and Impact on Exciton−Phonon Interaction. *ACS Cent. Sci.* **2019**, *5* (8), 1377−1386.

https://doi.org/10.1021/acsenergylett.2c00877
ACS Energy Lett. 2022, 7, 2745−2752